Study of the footprints of short-term variation in XCO_2 observed by TCCON sites using NIES and FLEXPART atmospheric transport models

D.A. Belikov[1,2,3,*], S. Maksyutov[1], A. Ganshin[3,4], R. Zhuravlev[3,4], N.M. Deutscher[5,6], D. Wunch[7], D.G. Feist[8], I. Morino[1], R. J. Parker[9], K. Strong[10], Y. Yoshida[1], A. Bril[11], S. Oshchepkov[11], H.Boesch[9], M. K. Dubey[12], D. Griffith[5], W. Hewson[9], R. Kivi[13], J. Mendonca[10], J. Notholt[6], M. Schneider[14], R. Sussmann[15], V.A. Velazco[5], and S. Aoki[16]

[1]{National Institute for Environmental Studies, Tsukuba, Japan}

[2]{National Institute of Polar Research, Tokyo, Japan}

[3]{Tomsk State University, Tomsk, Russia}

[4]{Central Aerological Observatory, Dolgoprudny, Russia}

[5]{Centre for Atmospheric Chemistry, School of Chemistry, University of Wollongong, Wollongong, NSW, Australia}

[6]{Institute of Environmental Physics, University of Bremen, Bremen, Germany}

[7]{California Institute of Technology, Pasadena, CA, USA}

[8]{Max Planck Institute for Biogeochemistry, Jena, Germany}

[9]{Earth Observation Science, University of Leicester, Leicester, UK}

[10]{Department of Physics, University of Toronto, Toronto, ON, Canada}

[11]{Institute of Physics of the National Academy of Sciences, Minsk, Belarus}

[12]{Earth System Observations, Los Alamos National Laboratory, Los Alamos, New Mexico}

[13]{Finnish Meteorological Institute, Sodankylä, Finland}

[14]{Agencia Estatal de Meteorolog´ıa (AEMET), CIAI, Santa Cruz de Tenerife, Spain}

[15]{Karlsruhe Institute of Technology, IMK-IFU, Garmisch-Partenkirchen, Germany}

[16]{Tohoku University, Sendai, Japan}

* {Currently at Hokkaido University, Sapporo, Japan}

Correspondence to: D. A. Belikov (dmitry.belikov@nies.go.jp)

1   Abstract

2   The Total Carbon Column Observing Network (TCCON) is a network of ground-based
3   Fourier Transform Spectrometers (FTS) that record near-infrared (NIR) spectra of the Sun.
4   From these spectra, accurate and precise observations of CO_2 column-averaged dry-air mole
5   fraction (denoted XCO_2) are retrieved. TCCON FTS observations have previously been used to
6   validate satellite estimations of XCO_2; however, our knowledge of the short-term spatial and
7   temporal variations in XCO_2 surrounding the TCCON sites is limited.

8   In this work, we use the National Institute for Environmental Studies (NIES) Eulerian
9   three-dimensional transport model and the FLEXPART (FLEXible PARTicle) Lagrangian
10   Particle Dispersion Model (LPDM) to determine the footprints of short-term variations in
11   XCO_2 observed by operational, past, future, and possible TCCON sites. We propose a footprint-
12   based method for the colocation of satellite and TCCON XCO_2 observations, and estimate the
13   performance of the method using the NIES model and five GOSAT XCO_2 product datasets.
14   Comparison of the proposed approach with a standard geographic method shows higher
15   number of colocation points and average bias reduction up to 0.15 ppm for a subset of 16
16   stations for the period from January 2010 to January 2014. Case studies of the Darwin and La
17   Réunion sites reveal that when the footprint area is rather curved, non-uniform and
18   significantly different from a geographical rectangular area, the differences between these
19   approaches are more noticeable. This emphasizes that the colocation is sensitive to local
20   meteorological conditions and flux distributions.

22   **Keywords:** XCO_2, TCCON, GOSAT, atmospheric transport

1. Introduction

Satellite observations of the column-averaged dry-air mole fraction of CO_2 (XCO_2) have the potential to significantly advance our knowledge of carbon dioxide (CO_2) distributions globally and provide new information on regional CO_2 sources and sinks. Observations of XCO_2 are available from space-based instruments such as the SCanning Imaging Absorption SpectroMeter for Atmospheric CHartographY (SCIAMACHY; data available for period 2002-2012; Bovensmann et al., 1999), the Greenhouse gases Observing Satellite (GOSAT; data available since 2009; Kuze et al., 2009, 2016; Yokota et al., 2009), and the Orbiting Carbon Observatory-2 (OCO-2; available since middle 2014; Crisp et al., 2004). These satellites provide unprecedented spatial coverage of the variability in XCO_2 around the world, with the exception of polar regions and areas with dense clouds. These observations are, however, limited by the orbit of the satellites, which typically measure in the local afternoon.

Ground-based Fourier Transform Spectrometer (FTS) observations available from the Total Carbon Column Observing Network (TCCON) (Wunch et al., 2011, 2015) provide dense temporal resolution and are more precise and accurate than space-based instruments. However, the number of ground-based FTS sites is limited, with just 23 operational sites and several approved for the future. These sites are sparsely distributed, and Siberia, Africa, South America, and the oceans from middle to high latitudes are poorly covered. Despite this limitation, FTS observations are used to validate satellite retrievals in order to assess bias, variability, and other key parameters (e.g., Wunch et al., 2011; Lindqvist et al., 2015).

The spatial and temporal coverage of satellite observations over TCCON sites is sparse due to cloud and aerosol filters, retrieval selection criteria, and post-retrieval data quality filters. To obtain satellite observation data with small uncertainties it is necessary to apply a colocation method for aggregating neighboring soundings. Currently available methods for XCO_2 colocation include geographical (e.g., Cogan et al., 2012; Inoue et al., 2013; Reuter et al., 2013), T700 (it implies that the air with the same history of transport derived from the 700 hPa potential temperature has the same XCO_2; Wunch et al., 2011), model-based (Guerlet et al., 2013), and geostatistical approaches (Nguyen et al., 2014).

In the geographical colocation method a spatial region around a TCCON site is selected together with a temporal window for selecting the satellite data. Inoue et al. (2013) used daily mean observations within a 10° × 10° area, Reuter et al. (2013) selected the monthly median of all observations within a 10° × 10° area, and Cogan et al. (2012) implemented narrower limits, using a two-hour mean period within a ±5° × ±5° area.

To increase the number of soundings, the spatial region may be expanded and additional selection criteria imposed. In the T700 colocation method proposed by Wunch et al. (2011), all observations within ±30° longitude, ±10° latitude, and ±2 K of the selected TCCON location and within ±5 days window are employed.

The model-based method proposed by Oshchepkov et al. (2012) and improved by Guerlet et al. (2013) uses daily mean values within 0.5 ppm of the 3 day-averaged model XCO_2 values and located within ±25° longitude and ±7.5° latitude of a TCCON site.

Nguyen et al. (2014) developed a geostatistical colocation methodology that selects observations using a "distance" function, which is a modified Euclidian distance in terms of latitude, longitude, time, and mid-tropospheric temperature at 700 hPa.

The majority of colocation methods described above have a common disadvantage; i.e., they work with a rectangular spatial domain, which is convenient for technical handling but does not reflect the impact of surface sources or sinks of CO_2 and the local meteorology in the area of interest. The spatial domains in colocations should take into account these features to ensure that only appropriate observations are selected. Keppel-Aleks et al. (2011, 2012) showed that the largest gradient in XCO_2 is formed mainly by the north–south flux distribution, with variations in XCO_2 caused mainly by large-scale advection. TCCON and satellite XCO_2 observations have pronounced temporal variability and are thus important in studies of short-term variations in XCO_2.

In this paper we study short-term variations in XCO_2 observed at TCCON sites. Although the XCO_2 is derived from column-averaged concentrations of CO_2, XCO_2 observations are most sensitive to near-surface fluxes. The XCO_2 variations are thus related to changes in the CO_2 mole fraction occurring near the surface surrounding the TCCON sites (hereafter known as the footprints of the TCCON sites).

The remainder of this paper is organized as follows: an overview of the method for estimating the footprints of TCCON sites is presented in Section 2. The results of the footprint estimation and a new method for colocation are presented and discussed in Sections 3,4, and the conclusions are given in Section 5.

2. Method

To estimate the footprints of TCCON sites we used forward simulations employing the NIES Eulerian three-dimensional transport model (TM) and backward trajectory tracking using the FLEXPART LPDM model.

The key features of the NIES TM are as follows: a reduced horizontal latitude–longitude grid with a spatial resolution of 2.5° × 2.5° near the equator (Belikov et al., 2011); a vertical flexible hybrid sigma–isentropic (σ–θ) grid with 32 levels up to the level of 5 hPa (Belikov et al., 2013b); separate parameterization of the turbulent diffusivity in the PBL and free troposphere (provided by the European Centre for Medium-Range Weather Forecasts (ECMWF) ERA-Interim reanalysis); and a modified Kuo-type parameterization scheme for cumulus convection (Belikov et al., 2013a).

The NIES model has previously been used to study the seasonal and inter-annual variability in CO_2. Belikov at al. (2013b) reported that the NIES model is able to successfully reproduce the vertical profile of CO_2 as well as the seasonal and inter-annual variability in XCO_2. A comparison of modeled output with TCCON observations (Belikov et al., 2013b) revealed model biases of ±0.2% for XCO_2; on this basis we assume that the NIES TM is able to successfully reproduce the vertical profile of CO_2 at the locations of TCCON sites.

Firstly we run NIES TM for the target period (January 2010 to February 2011) using ten year's spin-up to ensure reduction of initialization errors. Then NIES TM CO_2 concentrations sampled at the location of TCCON sites at the level of 1 km above ground at 13:00 local time were used to initialize backward tracer simulations with the FLEXPART model. FLEXPART, like other Lagrangian Particle Dispersion Models (LPDMs), considers atmospheric tracers as a discrete phase and tracks the pathway of each individual particle back in time until intersection with the Earth surface (Stohl et al., 2009). Obtained FLEXPART simulation results were then used to identify the areas in which TCCON soundings are most sensitive to variations.

The level of 1 km above ground typically corresponds to the top of the daytime planetary boundary layer (PBL). The PBL is the lowest part of the atmosphere and its behavior is directly influenced by its contact with the planetary surface. Turbulence causes intensive vertical mixing of the air within the PBL, so CO_2 released from the surface is roughly uniformly distributed throughout the column of air in the PBL at local noon, when the maximum extent of vertical mixing occurs. The selected sampling time is also favorable for minimizing errors in the initial CO_2 concentration calculated by NIES TM, as this type of chemical transport model has proved to be successful in resolving the diurnal vertical profiles of tracers (Belikov et al., 2013a).

To run NIES TM and FLEXPART model we use fluxes obtained with the GELCA-EOF (Global Eulerian-Lagrangian Coupled Atmospheric model with Empirical Orthogonal

Function) inverse modeling scheme (Zhuravlev et al., 2013). A priori fluxes consist of four types: 1) the Open source Data Inventory of Anthropogenic CO_2 (ODIAC) (Oda et al., 2011) and the Carbon Dioxide Information Analysis Center's (CDIAC) (Andres et al., 2011) anthropogenic fluxes; 2) the Vegetation Integrative SImulator for Trace gases (VISIT) (Ito, 2010) biosphere fluxes; 3) the Offline ocean Tracer Transport Model (OTTM) (Valsala et al., 2013) oceanic fluxes; and 4) the Global Fire Emissions Database (GFED) (Van der Werf et al., 2010) biomass burning emissions. Both models are driven by the Japanese Meteorological Agency Climate Data Assimilation System (JCDAS) datasets (Onogi et al., 2007).

Variations in TCCON XCO_2 are influenced by a large scale processes. Keppel-Aleks et al. (2012) presented a robust relationship between weekly and monthly aggregated total column CO_2 and local net ecosystem exchange, while column drawdown has only a weak correlation with the regional flux on daily timescales. Thus the maximum trajectory duration for the FLEXPART was therefore set to one week. The FLEXPART model was run with resolution of 1 degree and 2 h time step for a 14-month period from January 2010 to February 2011.

3. Results

3.1. Sensitivity of TCCON site footprints

We analyzed two groups of TCCON sites: operational sites (Table 1; Figs. 1 and 2) and past, future, and possible sites (Table 2; Fig. 3). We included Arrival Heights (Antarctica) and Yekaterinburg (Russia) in the second group, though the status of these monitoring stations is unclear. The footprint estimation is restricted to the summer season for high-latitude sites (Arrival Heights, Eureka, Ny Ålesund, Poker Flat, and Sodankylä), due to limitations relating to the solar zenith angle.

3.1.1.   Operational sites

North America

The five active American sites are located in the US and Canada, so they are sensitive to the western and central part of North America, the northern part of Canada and Greenland, and the eastern part of the Pacific Ocean. There are no TCCON sites in Alaska or on the east coast of North America, which is a region of intense anthropogenic activity (Fig. 1).

European sites

The European region contains eight operational sites (Fig. 2). We also include Izaña, which does not belong to this region but is located very close to it. This region has a good spatial coverage of operational TCCON sites; however, most sites are located near the coast and are thus very sensitive to the Atlantic and Arctic oceans. The maximum footprint sensitivity occurs in western Europe where there is a high density of operational TCCON sites; five sites (Bremen, Garmisch, Karlsruhe, Orléans, and Paris) are concentrated within a small area. The sensitivity decreases quite rapidly towards the east and south, and only parts of eastern Europe and north Africa are covered.

Asia

The footprints of Asian sites mainly span countries bordering the Sea of Japan; i.e., Japan, Korea, the Russian Far East, and east China. These sites are also able to capture signals from Mongolia, eastern Siberia, and Southeast Asia. Although the coverage of these sites is relatively small, the main industrial centers in the region are included.

Australia and New Zealand

The footprint sensitivity of TCCON sites in this region covers almost all of Australia. Chevallier et al. (2011) shows TCCON data could constrain flux estimates over Australia equally well as the existing in situ measurements. Our footprint estimations are, however, more sensitive to the ocean regions between Australia and New Zealand as well as adjacent coastal areas.

Oceanic sites: Ascension Island and La Réunion Island

Ascension Island is in the Trade Wind belt of the tropical Atlantic, ideally located to measure the South Atlantic marine boundary layer. The South East Trade Winds, which are almost invariant and are derived from the deep South Atlantic Ocean with little contact with Africa. Surface measurements of CO_2 at Ascension Island are used as a background (Gatti et al., 2010). However, above the Trade Wind Inversion (TWI), at about 1200–2000 m above sea level, the air masses are very different, coming dominantly from tropical Africa and occasionally South America (Swap et al., 1996). The FLEXPART simulation with tracers released at an altitude of 3000 m detected some hotspots in Africa (Fig. 1b). The study of biomass burning in Africa is essential, but lies outside of the scope of this paper.

La Réunion island situated in the Indian Ocean at about 800 km east of Madagascar. For this site the seasonal trend of wind mainly remains in the easterly sector, so the footprint covers mainly ocean regions. La Réunion site is further discussed in Section 4.3.2.

3.1.2. Past, future, and possible TCCON sites

The footprints of past, future, and possible TCCON sites are presented in Fig. 3. The Oxfordshire site enhances the sensitivity of the region, which is already well covered by existing TCCON sites in Europe. The East Trout Lake, Four Corners, and Poker Flat sites fill sensitivity gaps in the Canadian Boreal forest, the southwestern US, northern Mexico, and Alaska. Nevertheless, there are no TCCON sites near the Atlantic coast of North America, which is a key region of interest.

In South America, the Manaus site (briefly in operation during 2014 and will operate after reconstruction) was ideally located in central Amazonia. However, meteorological conditions meant that a signal was only detected in a very narrow section towards the east. Observations at this site are more sensitive to anthropogenic activity on the Atlantic coast of South America, compared with the surrounding Amazonian biosphere. Additional use of CO

observations will be necessary to isolate the Net Primary Production signal in Central Amazonia (Keppel-Aleks et al., 2012). Another site in this region is Paramaribo located in Suriname which is part of Caribbean South America. The footprint of the Paramaribo site is narrowly focused towards the Atlantic Ocean due to site location and meteorological conditions as stated above.

Burgos in the northern Philippines extends the Asian footprint southward. The location of the Yekaterinburg site is ideal, as it quite evenly covers a large area of western Russia. The site reduces the gap between the European and Asian TCCON domains. The Arrival Heights site is located on the Antarctic coast and currently cannot be used for satellite data validation. Given the air circulation near the South Pole, this site can be useful for measuring the background value of XCO_2.

In general, the operational stations cover some regions well (North America, Europe, the Far East, Southeast Asia, Australia, and New Zealand), and the planned sites will improve this coverage. However, on a global scale there are major gaps that highlight the difficulty in generalizing the available data along latitude for bias correction.

The short-term variations in CO_2 in the near surface and free troposphere (<3000 m) have the same form, but different intensity (Fig. 1b), as a smaller number of tracers from the middle troposphere reached the surface during the simulation time.

3.2. Seasonal variability in footprints

Some TCCON stations have strong seasonal variations in their footprint due to changes in wind direction; i.e., Białystok, Darwin, Izaña, Park Falls, and Tsukuba (Fig. 4). For other sites (e.g., Ascension and Manaus) the weather conditions are less variable throughout the year. The depth of the PBL changes with season and is thus an important factor that influences the footprint. In winter the PBL lowers, causing less vertical mixing and enhancing horizontal tracer transport; this leads to a wider spatial coverage of the footprints.

4. Applying the model-derived footprints to the colocation of XCO2

In the next two sections we assess the performance of the footprint-based method of colocating TCCON XCO_2 against the NIES model and GOSAT product datasets. The colocation domain size for each site is determined by sensitivity values (ppm (μmol (m^{2}s)$^{-1}$)$^{-1}$) with the limits of $\log_{10}(x)$ equal to −0.5, −1.0, −1.5, and −2.0 (cases C1-C4). These sensitivity values were selected to approximately correspond to the domain sizes in standard geographical

colocation techniques, which have rectangular dimensions of 2.5° × 2.5°, ±5.0° × ±5.0°, ±5.0° × ±10.0°, and ±7.5° × ±22.5° (cases C5-C8). Only coincident observations were used, and observations with differences of ≥3 ppm were discarded from the comparison. Considered period for comparison is January 2010 and January 2014.

TCCON observations were used from 16 sites: Białystok, Caltech, Darwin, Eureka, Garmisch, Izaña, Karlsruhe, Lamont, Lauder (125HR), Orléans, Park Falls, La Réunion Island, Saga, Sodankylä, Tsukuba (125HR), and Wollongong. These observations were obtained from the 2014 release of TCCON data ("GGG2014"), available from the TCCON Data Archive (http://tccon.ornl.gov).

4.1. Colocation of XCO_2 from TCCON and the NIES model

The TCCON and NIES TM datasets are initially compared using a geographical colocation of 2.5° × 2.5° that corresponds to selecting the nearest NIES TM cell (Table 3). The resolution of the model grid is rather coarse, so we observe that the results depend mainly on the size of the colocation area but not on the form. With increasing size of the colocation area the correlation between XCO_2 from TCCON and NIES TM slightly increases from 0.96 to 0.97 and the standard deviation decreases from 1.1 to 0.96 ppm. This is due to an increase in the number of observations, which results in a larger average bias.

For Darwin, Eureka, Izaña, Lauder, La Réunion, Sodankylä, and Wollongong, the residuals between the datasets are small and similar for all methods (see Fig. 5a for Darwin; cases C1, C4, C5, and C8). Here, XCO_2 is under the influence of global long-term variations that are included in the NIES TM. The low sensitivity of the model to local sources does not cause a significant difference between the colocation methods. For the second group (non-operational sites), local sources are essential and even coarse-grid models can capture their signal. As a result, the shape of the colocation area is important (see Fig. 5b for Garmisch; cases C1, C4, C5, and C8).

4.2. Colocation of XCO_2 from TCCON and GOSAT products

A comparison of colocation methods was performed for five GOSAT XCO_2 products: NIES v02.11 (Yoshida et al., 2013) and PPDF-S v02.11 from the NIES, Japan (Oshchepkov et al., 2013); ACOS B3.4 from the NASA Atmospheric CO_2 Observations from Space (ACOS) team (O'Dell et al., 2012); RemoTeC v2.11 from the Netherlands Institute for Space Research/Karlsruhe Institute of Technology, Germany (Butz et al., 2011; Guerlet et al., 2013); and UoL-FP v4 from the University of Leicester, UK (Boesch et al., 2011; Cogan et al., 2012).

The results of the comparison of eight colocation methods employed for the five GOSAT XCO$_2$ products are presented in Tables 4–8. Only coincident observations were used, and observations with differences of ≥3 ppm were discarded from the comparison. The number of observations selected for colocation between the methods with the smallest areas (C1 and C5) and largest areas (C4 and C8) differs by approximately a factor of 5. There is, however, no clear dependence of the colocation efficiency on the number of observations. The correlation coefficient and standard deviation are within 0.81–0.93 and 1.02–1.22 ppm, respectively, regardless of the method used. Mean bias values are within 0.50–0.87 ppm, with the footprint method typically having a slightly lower bias by 0.02–0.15 ppm and higher number of colocations. For individual stations, these statistics may lie slightly outside the specified ranges.

4.3. Case study

In this section we demonstrate the developed colocation method for GOSAT observations over the Darwin and La Réunion Island TCCON sites.

4.3.1. Darwin site

The Northern Territory of Australia has two distinctive climate zones: the northern and southern. The northern zone, including Darwin, has three distinct seasons: the dry season (May to September), the build-up season (high humidity, but little rain: October to December) and the wet season associated with tropical cyclones and monsoon rains (December to April). The average maximum temperature is remarkably similar all year round. The southern zone is mainly desert with a semi-arid climate and little rain. To the north of Darwin, the territory is bordered by the Timor Sea, the Arafura Sea, and the Gulf of Carpentaria. The Northern Territory therefore has a pronounced seasonal variability that affects the spatial and temporal distribution of CO$_2$ and thus the footprint (Figs 4 and 6a).

Figures 6b and 6c show the locations of GOSAT observations selected using a geographical method within an area of ±7.5° × ±22.5° and a footprint-based method with the limit $\log_{10}(x) = -2.0$. Sizes of selected colocation areas (C4 and C8 methods) are close to ones used in others works (Wunch et al., 2011, Guerlet et al., 2013, Inoue et al. 2013, Reuter et al. 2013, Nguyen et al., 2014).

For ACOS, NIES, and RemoTeC GOSAT products the distributions of XCO$_2$ datasets for the Darwin site are similar and cover an area to the west of Darwin, including ground-based

observations from central Australia (Fig. 6c). The comparison of colocation methods shows the footprint-based method (C4) outperforms the geographical method (C8) for these three GOSAT products (Fig. 7), with approximately 3 times as many observations.

Although currently the UoL GOSAT XCO_2 version 6 includes ocean-glint observations, in this study we use slightly outdated the UoL-FP GOSAT product v4, which has only overland points. In this case the difference between colocations subsets is the observations towards the south over land, which provide a similar distribution as the ACOS product, but without marine observations (Fig. 6b and Fig. 6c). These differences in the covered areas have a significant negative effect on the result (Fig. 7). From that it can be concluded that XCO_2 patterns towards the south over land are rather different from those around Darwin, the sun-glint observation over the ocean are important and must be included into analysis. Thus, XCO_2 at the Darwin site is under the influence of the three different fluxes coming from surrounding land area, central part of Australia and oceanic regions. The oceanic observation over the Coral sea is quite important, though substantially removed from the station.

4.3.2. La Réunion site

La Réunion is a small island east of Madagascar surrounded by the Indian Ocean. The nearest land territory to La Réunion is Mauritius, located ~175 km to the northwest. The meteorological conditions in the region mean that the footprint of the La Réunion site mostly covers a large area of ocean to the southeast of the island and a small area of northern Madagascar (Fig. 8).

The geographical colocation method does not take into account local conditions. Therefore, despite the fact that the site is predominantly oceanic, the geographical method includes observations made over land in Madagascar and the southeast coast of Africa (Fig. 8b). In contrast, the footprint method takes into account the local meteorology, so observations are predominantly taken from the ocean (Fig. 8c). Since the UoL-FP dataset has no observations over the sea, the observations for this dataset are located only over Madagascar (Fig. 9).

Unlike Darwin, La Réunion receives clean air from the ocean and thus has very little CO_2 variation. The selection of areas for colocation therefore did not reveal any significant advantages of the footprint-based method, with the exception of a slightly smaller bias for the NIES and RemoTec products (Fig. 10). The comparison of the UoL-FP product for method C4 and method C8 shows that the XCO_2 cycles over Madagascar and the eastern coast of Africa

are quite different (Fig. 10). This highlights that the exclusion of marine observations leads to poor results over marine-based TCCON sites.

A comparison of TCCON data and NIES model results for Darwin and La Réunion shows that XCO_2 for these sites is controlled mainly by large-scale changes. However, analysis of GOSAT products emphasizes that the influence of local sources is also important. The geographical method of colocation assumes a fairly even distribution of GOSAT observations near TCCON sites, while the calculated footprints have strongly curved shapes and an uneven distribution. We therefore expect the proposed footprint method to be useful for other sites with rather curved and non-uniform footprints, such as the Ascension Island and Manaus sites.

5. Summary

We have developed a method for assessing the footprints of short-term XCO_2 variations observed by TCCON ground-based FTS sites. The method is based on one-week FLEXPART backward trajectory simulations that are initiated at an altitude of 1 km (the upper border of the PBL) in the afternoon using the vertical CO_2 distribution calculated by the NIES transport model.

We applied this method to estimate footprints of the operational, past, future, and possible TCCON sites, and revealed some basic patterns. Most sites located near coastal regions are strongly influenced by ocean regions; thus, there is a large seasonal variability in footprints for Białystok, Darwin, Izaña, Park Falls, and Tsukuba. The Ascension Island, Manaus, and La Réunion sites have very narrow footprints that show small seasonal variations.

We proposed the footprint-based method for the colocation of satellite observations with TCCON sites, and assessed the performance of the method using the NIES model and GOSAT product datasets. The colocation footprint area is determined by yearly averaged sensitivity values with limits of $\log_{10}(x)$ equals −0.5, −1.0, −1.5 and −2.0. These were selected to approximately correspond to the areas of standard geographical colocation techniques that have rectangular shapes of 2.5° × 2.5°, ±5.0° × ±5.0°, ±5.0° × ±10.0°, and ±7.5° × ±22.5°, respectively. Comparison of the proposed method with the geographical method showed similar but smaller biases for a subset of 16 stations for the period from January 2009 to January 2014. Case studies of the Darwin and La Réunion TCCON sites revealed that the footprint has a very different colocation area to that of the geographical method, especially

near marine coast.

This study shows the use of colocation methods similar to geographical, which are based on tracking long-term trends of tracers (i.e. derived from global model calculations) has its limitations and works up to a certain accuracy threshold, after which it is impossible to ignore the influence of local sources. Given that the GOSAT XCO_2 products are sensitive to local sources, proposed footprint method is promising and requires further fine-tuning. The potential for further improvement includes moving from gross annual averaging to more accurate seasonal or monthly averaging. In addition, it is possible to study the sensitivity of XCO_2 observations using adjoint of the global Eulerian–Lagrangian coupled atmospheric transport model (Belikov et al., 2016), which can resolve long-term, synoptic and hourly variation patterns.

We believe, however, that the footprint analysis should be considered important in the appraisal of new TCCON sites, along with assessments of the number of cloudless days, the surrounding landscape, and the reflectivity of the Earth's surface.

Acknowledgments

Authors thank Paul Wennberg for insightful discussions and suggestions regarding the manuscript.

The JRA-25/JCDAS meteorological datasets used in the simulations were provided by the Japan Meteorological Agency. The computational resources were provided by NIES. This study was performed by order of the Ministry for Education and Science of the Russian Federation No. 5.628.2014/K and was supported by The Tomsk State University Academic D.I. Mendeleev Fund Program in 2014–2015 and by the GRENE Arctic project.

TCCON data were obtained from the TCCON Data Archive, hosted by the Carbon Dioxide Information Analysis Center (CDIAC) at Oak Ridge National Laboratory, Oak Ridge, Tennessee, U.S.A., http://tccon.ornl.gov. The Ascension Island site has been funded by the Max Planck Society. The Bremen, Białystok, and Orléans TCCON sites are funded by the EU projects InGOS and ICOS-INWIRE, and by the Senate of Bremen. The Darwin and Wollongong TCCON sites are funded by NASA grants NAG5-12247 and NNG05-GD07G, and Australian Research Council grants DP140101552, DP110103118, DP0879468, LE0668470, and LP0562346. We are grateful to the DOE ARM program for technical support at the Darwin TCCON site. Nicholas Deutscher was supported by an Australian Research Council fellowship, DE140100178.

The Eureka measurements were made at the Polar Environment Atmospheric Research Laboratory (PEARL) by the Canadian Network for the Detection of Atmospheric Change (CANDAC) led by James R. Drummond, and in part by the Canadian Arctic ACE Validation Campaigns led by Kaley A. Walker. They were supported by the AIF/NSRIT, CFI, CFCAS, CSA, EC, GOC-IPY, NSERC, NSTP, OIT, ORF, and PCSP.

The University of Leicester data were obtained with funding from the UK National Centre for Earth Observation and the ESA GHG-CCI project, using the ALICE High Performance Computing Facility at the University of Leicester. R. Parker was funded by an ESA Living Planet Fellowship.

1 References

Andres, R. J., Gregg, J. S., Losey, L., Marland, G., and Boden, T.: Monthly, global emissions of carbon dioxide from fossil fuel consumption, Tellus, 63B, 309–327, 2011.

Belikov, D., Maksyutov, S., Miyasaka, T., Saeki, T., Zhuravlev, R., and Kiryushov, B.: Mass-conserving tracer transport modelling on a reduced latitude–longitude grid with NIES-TM, Geosci. Model Dev., 4, 207–222, 2011.

Belikov, D. A., Maksyutov, S., Krol, M., Fraser, A., Rigby, M., Bian, H., Agusti-Panareda, A., Bergmann, D., Bousquet, P., Cameron-Smith, P., Chipperfield, M. P., Fortems-Cheiney, A., Gloor, E., Haynes, K., Hess, P., Houweling, S., Kawa, S. R., Law, R. M., Loh, Z., Meng, L., Palmer, P. I., Patra, P. K., Prinn, R. G., Saito, R., and Wilson, C.: Off-line algorithm for calculation of vertical tracer transport in the troposphere due to deep convection, Atmos. Chem. Phys., 13, 1093–1114, doi:10.5194/acp-13-1093-2013, 2013a.

Belikov, D., Maksyutov, S., Sherlock, V., Aoki, S., Deutscher, N. M., Dohe, S., Griffith, D., Kyro, E., Morino, I., Nakazawa, T., Notholt, J., Rettinger, M., Schneider, M., Sussmann, R., Toon, G. C., Wennberg, P. O., and Wunch, D.: Simulations of column-average CO_2 and CH_4 using the NIES TM with a hybrid sigma–isentropic (σ–ϑ) vertical coordinate, Atmos. Chem. Phys., 13, 1713–1732, doi:10.5194/acp-13-1713-2013, 2013b.

Belikov, D. A., Maksyutov, S., Yaremchuk, A., Ganshin, A., Kaminski, T., Blessing, S., Sasakawa, M., Gomez-Pelaez, A. J., and Starchenko, A.: Adjoint of the global Eulerian–Lagrangian coupled atmospheric transport model (A-GELCA v1.0): development and validation, Geosci. Model Dev., 9, 749-764, doi:10.5194/gmd-9-749-2016, 2016.

Boesch, H., Baker, D., Connor, B., Crisp, D., and Miller, C.: Global characterization of CO_2 column retrievals from shortwave-infrared satellite observations of the Orbiting Carbon Observatory-2 Mission, Remote Sens., 3, 270–304, doi:10.3390/rs3020270, 2011.

Bovensmann, H., Burrows, J. P., Buchwitz, M., Frerick, J., Noël, S., Rozanov, V. V., Chance, K. V., and Goede, A. P. H.: SCIAMACHY: Mission objectives and measurement modes, J. Atmos. Sci., 56, 127–150, 1999.

Butz, A., Guerlet, S., Jacob, D. J., Schepers, D., Galli, A., Aben, I., Frankenberg, C., Hartmann, J.-M., Tran, H., Kuze, A., Keppel-Aleks, G., Toon, G. C., Wunch, D., Wennberg, P. O., Deutscher, N. M., Griffith, D. W. T., Macatangay, R., Messerschmidt, J., Notholt, J., and Warneke, T.: Toward accurate CO_2 and CH_4 observations from GOSAT, Geophys. Res. Lett., 38, 2–7, 2011.

Chevallier, F., Deutscher, N. M., Conway, T. J., Ciais, P., Ciattaglia, L., Dohe, S., Frohlich, M., Gomez-Pelaez, A. J., Griffith, D., Hase, F., Haszpra, L., Krummel, P., Kyro, E., Labuschagne, C., Langenfelds, R., Machida, T., Maignan, F., Matsueda, H., Morino, I., Notholt, J., Ramonet, M., Sawa, Y., Schmidt, M., Sherlock, V., Steele, P., Strong, K., Sussmann, R., Wennberg, P., Wofsy, S., Worthy, D., Wunch, D., and Zimnoch, M.: Global CO_2 fluxes inferred from surface air-sample measurements and from TCCON retrievals of the CO2 total column, Geophys. Res. Lett., 38, L24810, doi:10.1029/2011GL049899, 2011

1   Cogan, A. J., Boesch, H., Parker, R. J., Feng, L., Palmer, P. I., Blavier, J.-F. L., Deutscher, N. M.,
2   Macatangay, R., Notholt, J., Roehl, C., Warneke, T., and Wunch, D.: Atmospheric
3   carbon dioxide retrieved from the Greenhouse gases Observing SATellite (GOSAT):
4   Comparison with ground-based TCCON observations and GEOS-Chem model
5   calculations, J. Geophys. Res. Atmos., 117, D21301, doi:10.1029/2012JD018087, 2012.
6   Crisp, D., Atlas, R. M., Bréon, F.-M., Brown, L. R., Burrows, J. P., Ciais, P., Connor, B. J., Doney,
7   S. C., Fung, I. Y., Jacob, D. J., Miller, C. E., O'Brien, D., Pawson, S., Randerson, J. T.,
8   Rayner, P., Salawitch, R. S., Sander, S. P., Sen, B., Stephens, G. L., Tans, P. P., Toon, G.
9   C., Wennberg, P. O., Wofsy, S. C., Yung, Y. L., Kuang, Z., Chudasama, B., Sprague, G.,
10   Weiss, P., Pollock, R., Kenyon, D., and Schroll, S.: The Orbiting Carbon Observatory
11   (OCO) mission, Adv. Space Res., 34, 700–709, 2004.
12   Deutscher, N. M., Griffith, D. W. T., Bryant, G. W., Wennberg, P. O., Toon, G. C.,
13   Washenfelder, R. A., Keppel-Aleks, G., Wunch, D., Yavin, Y., Allen, N. T., Blavier, J.-F.,
14   Jiménez, R., Daube, B. C., Bright, A. V., Matross, D. M., Wofsy, S. C., and Park, S.: Total
15   column CO_2 measurements at Darwin, Australia-site description and calibration against
16   in situ aircraft profiles, Atmos. Meas. Tech., 3, 947-958, doi:10.5194/amt-3-947-2010,
17   2010.
18   Gatti, L. V., Miller, J. B., D'Amelio, M. T. S., Martinewski, A., Basso, L. S., Gloor, M. E., Wofsy,
19   S., and Tans, P.: Vertical pro- files of CO_2 above eastern Amazonia suggest a net carbon
20   flux to the atmosphere and balanced biosphere between 2000 and 2009, Tellus B, 62,
21   581–594, doi:10.1111/j.1600-0889.2010.00484.x, 2010.
22   Geibel, M. C., Gerbig, C., and Feist, D. G.: A new fully automated FTIR system for total
23   column measurements of greenhouse gases, Atmos. Meas. Tech., 3, 1363-1375,
24   doi:10.5194/amt-3-1363-2010, 2010.
25   Guerlet, S., Butz, A., Schepers, D., Basu, S., Hasekamp, O. P., Kuze, A., Yokota, T., Blavier, J.-
26   F., Deutscher, N. M., Griffith, D. W., Hase, F., Kyro, E., Morino, I., Sherlock, V.,
27   Sussmann, R., Galli, A., and Aben, I.: Impact of aerosol and thin cirrus on retrieving and
28   validating XCO_2 from GOSAT shortwave infrared measurements, J. Geophys. Res.
29   Atmos., 118, 4887–4905, 2013.
30   Inoue, M., Morino, I., Uchino, O., Miyamoto, Y., Yoshida, Y., Yokota, T., Machida, T., Sawa, Y.,
31   Matsueda, H., Sweeney, C., Tans, P. P., Andrews, A. E., Biraud, S. C., Tanaka, T.,
32   Kawakami, S., and Patra, P. K.: Validation of XCO_2 derived from SWIR spectra of GOSAT
33   TANSO-FTS with aircraft measurement data, Atmos. Chem. Phys., 13, 9771–9788,
34   doi:10.5194/acp-13-9771-2013, 2013.
35   Ito, A.: Changing ecophysiological processes and carbon budget in East Asian ecosystems
36   under near-future changes in climate: Implications for long-term monitoring from a
37   process-based model, J. Plant Res., 123, 577–588, 2010.
38   Keppel-Aleks, G., Wennberg, P. O., and Schneider, T.: Sources of variations in total column
39   carbon dioxide, Atmos. Chem. Phys., 11, 3581–3593, doi:10.5194/acp-11-3581-2011,
40   2011.
41   Keppel-Aleks, G., Wennberg, P. O., Washenfelder, R. A., Wunch, D., Schneider, T., Toon, G.
42   C., Andres, R. J., Blavier, J.-F., Connor, B., Davis, K. J., Desai, A. R., Messerschmidt, J.,
43   Notholt, J., Roehl, C. M., Sherlock, V., Stephens, B. B., Vay, S. A., and Wofsy, S. C.: The

imprint of surface fluxes and transport on variations in total column carbon dioxide, Biogeosciences, 9, 875–891, doi:10.5194/bg-9-875-2012, 2012.

Kuze, A., Suto H., Nakajima M., and Hamazaki, T.: Thermal and near infrared sensor for carbon observation Fourier-transform spectrometer on the Greenhouse Gases Observing Satellite for greenhouse gases monitoring, Appl. Opt., 48, 6716–6733, doi:10.1364/AO.48.006716, 2009.

Kuze, A., suto, H., Shiomi, K., Kawakami, S., Tanaka, M., Ueda, Y., Deguchi, A., Yoshida, J., Yamamoto, Y., Kataoka, F., Taylor, T. E., and Buijs, H.: Update on GOSAT TANSO-FTS performance, operations, and data products after more than six years in space, Atmos. Meas. Tech. Discuss., doi:10.5194/amt-2015-333, in review, 2016.

Lindqvist, H., O'Dell, C. W., Basu, S., Boesch, H., Chevallier, F., Deutscher, N., Feng, L., Fisher, B., Hase, F., Inoue, M., Kivi, R., Morino, I., Palmer, P. I., Parker, R., Schneider, M., Sussmann, R., and Yoshida, Y.: Does GOSAT capture the true seasonal cycle of XCO_2?, Atmos. Chem. Phys. Discuss., 15, 16461–16503, doi:10.5194/acpd-15-16461-2015, 2015.

Messerschmidt, J., Macatangay, R., Notholt, J., Petri, C., Warneke, T., and Weinzierl, C.: Side by side measurements of CO2 by ground-based Fourier transform spectrometry (FTS), Tellus B, 62, 749–758, doi:10.1111/j.1600-0889.2010.00491.x, 2010.

Messerschmidt, J., Chen, H., Deutscher, N. M., Gerbig, C., Grupe, P., Katrynski, K., Koch, F.-T., Lavrič, J. V., Notholt, J., Rödenbeck, C., Ruhe, W., Warneke, T., and Weinzierl, C.: Automated ground-based remote sensing measurements of greenhouse gases at the Białystok site in comparison with collocated in situ measurements and model data, Atmos. Chem. Phys., 12, 6741–6755, doi:10.5194/acp-12-6741-2012, 2012.

Nguyen, H., Osterman, G., Wunch, D., O'Dell, C., Mandrake, L., Wennberg, P., Fisher, B., and Castano, R.: A method for collocating satellite XCO_2 data to ground-based data and its application to ACOS-GOSAT and TCCON, Atmos. Meas. Tech., 7, 2631–2644, doi:10.5194/amt-7-2631-2014, 2014.

Oda, T. and Maksyutov, S.: A very high-resolution (1 km × 1 km) global fossil fuel CO_2 emission inventory derived using a point source database and satellite observations of nighttime lights, Atmos. Chem. Phys., 11, 543–556, doi:10.5194/acp-11-543-2011, 2011.

O'Dell, C. W., Connor, B., Bösch, H., O'Brien, D., Frankenberg, C., Castano, R., Christi, M., Eldering, D., Fisher, B., Gunson, M., McDuffie, J., Miller, C. E., Natraj, V., Oyafuso, F., Polonsky, I., Smyth, M., Taylor, T., Toon, G. C., Wennberg, P. O., and Wunch, D.: The ACOS CO_2 retrieval algorithm – Part 1: Description and validation against synthetic observations, Atmos. Meas. Tech., 5, 99–121, doi:10.5194/amt-5-99-2012, 2012.

Ohyama, H., Morino, I., Nagahama, T., Machida, T., Suto, H., Oguma, H., Sawa, Y., Matsueda, H., Sugimoto, N., Nakane, H., and Nakagawa, K.: Column-averaged volume mixing ratio of CO_2 measured with ground-based Fourier transform spectrometer at Tsukuba, J. Geophys. Res., 114, D18303, doi:10.1029/2008JD011465, 2009.

Onogi, K., Tsutsui, J., Koide, H., Sakamoto, M., Kobayashi, S., Hatsushika, H., Matsumoto, T., Yamazaki, N., Kamahori, H., Takahashi, K., Kadokura, S., Wada, K., Kato, K., Oyama, R.,

Ose, T., Mannoji, N., and Taira, R.: The JRA-25 Reanalysis, J. Meteor. Soc. Japan, 85, 369–432, 2007.

Oshchepkov, S., Bril, A., Yokota, T., Morino, I., Yoshida, Y., Matsunaga, T., Belikov, D., Wunch, D., Wennberg, P. O., Toon, G. C., O'Dell, C. W., Butz, A., Guerlet, S., Cogan, A., Boesch, H., Eguchi, N., Deutscher, N. M., Griffith, D., Macatangay, R., Notholt, J., Sussmann, R., Rettinger, M., Sherlock, V., Robinson, J., Kyrö, E., Heikkinen, P., Feist, D. G., Nagahama, T., Kadygrov, N., Maksyutov, S., Uchino, O., and Watanabe, H.: Effects of atmospheric light scattering on spectroscopic observations of greenhouse gases from space: Validation of PPDF-based CO_2 retrievals from GOSAT, J. Geophys. Res., 117, 1–18, 2012.

Oshchepkov, S., Bril, A., Yokota, T., Yoshida, Y., Blumenstock, T., Deutscher, N. M., Dohe, S., Macatangay, R., Morino, I., Notholt, J., Rettinger, M., Petri, C., Schneider, M., Sussman, R., Uchino, O., Velazco, V., Wunch, D., and Belikov, D.: Simultaneous retrieval of atmospheric CO_2 and light path modification from space-based spectroscopic observations of greenhouse gases: methodology and application to GOSAT measurements over TCCON sites, Appl. Optics, 52, 1339–1350, 2013.

Patra, P. K., Houweling, S., Krol, M., Bousquet, P., Belikov, D., Bergmann, D., Bian, H., Cameron-Smith, P., Chipperfield, M. P., Corbin, K., Fortems-Cheiney, A., Fraser, A., Gloor, E., Hess, P., Ito, A., Kawa, S. R., Law, R. M., Loh, Z., Maksyutov, S., Meng, L., Palmer, P. I., Prinn, R. G., Rigby, M., Saito, R., and Wilson, C.: TransCom model simulations of CH_4 and related species: linking transport, surface flux and chemical loss with CH_4 variability in the troposphere and lower stratosphere, Atmos. Chem. Phys., 11, 12813–12837, doi:10.5194/acp-11-12813-2011, 2011.

Reuter, M., Bösch, H., Bovensmann, H., Bril, A., Buchwitz, M., Butz, A., Burrows, J. P., O'Dell, C. W., Guerlet, S., Hasekamp, O., Heymann, J., Kikuchi, N., Oshchepkov, S., Parker, R., Pfeifer, S., Schneising, O., Yokota, T., and Yoshida, Y.: A joint effort to deliver satellite retrieved atmospheric CO_2 concentrations for surface flux inversions: the ensemble median algorithm EMMA, Atmos. Chem. Phys., 13, 1771–1780, doi:10.5194/acp-13-1771-2013, 2013.

Stohl, A., Seibert, P., Arduini, J., Eckhardt, S., Fraser, P., Greally, B. R., Lunder, C., Maione, M., Mhle, J., O'Doherty, S., Prinn, R. G., Reimann, S., Saito, T., Schmidbauer, N., Simmonds, P. G., Vollmer, M. K., Weiss, R. F., and Yokouchi, Y.: An analytical inversion method for determining regional and global emissions of greenhouse gases: Sensitivity studies and application to halocarbons, Atmos. Chem. Phys., 9, 1597–1620, doi:10.5194/acp-9-1597-2009, 2009.

Swap, R., Garstang, M., Macko, S. A., Tyson, P. D., Maenhaut, W., Artaxo, P., Kållberg, P., and Talbot R.: The long-range transport of southern African aerosols to the tropical South Atlantic, J. Geophys. Res., 101(D19), 23777–23791, doi:10.1029/95JD01049, 1996.

Valsala, V., and Maksyutov, S.: Interannual variability of the air–sea CO_2 flux in the north Indian Ocean, Ocean Dynam., 63, 165–178, doi:10.1007/s10236-012-0588-7, 2013.

Van der Werf, G. R., Randerson, J. T., Giglio, L., Collatz, G. J., Mu, M., Kasibhatla, P. S., Morton, D. C., DeFries, R. S., Jin, Y., and Van Leeuwen, T. T.: Global fire emissions and

the contribution of deforestation, savanna, forest, agricultural, and peat fires (1997–2009), Atmos. Chem. Phys., 10, 11707–11735, doi:10.5194/acp-10-11707-2010, 2010.

Washenfelder, R., Toon, G., Blavier, J., Yang, Z., Allen, N., Wennberg, P., Vay, S., Matross, D., and Daube, B.: Carbon dioxide column abundances at the Wisconsin Tall Tower site, J. Geophys. Res, 111, D22305, doi:10.1029/2006JD007154, 2006.

Wunch, D., Toon, G.C., Blavier, J.-F.L., Washenfelder, R.A., Notholt, J., Connor, B.J., Griffith, D.W.T., Sherlock, V., and Wennberg, P.O.: The Total Carbon Column Observing Network, Phil. Trans. R. Soc. A 369, 2087–2112, doi:10.1098/rsta.2010.0240, 2011.

Wunch, D., Toon, G.C, Sherlock, V., Deutscher, N.M., Liu, C., Feist, D.G., and Wennberg, P.O. The Total Carbon Column Observing Network's GGG2014 Data Version. Technical report, Carbon Dioxide Information Analysis Center, Oak Ridge National Laboratory, Oak Ridge, Tennessee, U.S.A., 2015. doi:10.14291/tccon.ggg2014.documentation.R0/1221662.

Yokota, T., Yoshida, Y., Eguchi, N., Ota, Y., Tanaka, T., Watanabe, H., and Maksyutov, S.: Global concentrations of CO_2 and CH_4 retrieved from GOSAT: First preliminary results, SOLA, 5, 160–163, doi:10.2151/sola.2009-041, 2009.

Yoshida, Y., Kikuchi, N., Morino, I., Uchino, O., Oshchepkov, S., Bril, A., Saeki, T., Schutgens, N., Toon, G. C., Wunch, D., Roehl, C. M., Wennberg, P. O., Griffith, D. W. T., Deutscher, N. M., Warneke, T., Notholt, J., Robinson, J., Sherlock, V., Connor, B., Rettinger, M., Sussmann, R., Ahonen, P., Heikkinen, P., Kyrö, E., Mendonca, J., Strong, K., Hase, F., Dohe, S., and Yokota, T.: Improvement of the retrieval algorithm for GOSAT SWIR XCO_2 and XCH_4 and their validation using TCCON data, Atmos. Meas. Tech., 6, 1533–1547, doi:10.5194/amt-6-1533-2013, 2013.

Zhuravlev, R.V., Ganshin, A.V., Maksyutov, S.S., Oshchepkov, S.L., Khattatov, B.V.: Estimation of global fluxes of CO2 using ground-station and satellite (GOSAT) observation data with empirical orthogonal functions. Atmos. Oceanic Opt., 26, 388-397, 2013.

1   **Table 1.**   Details of operational TCCON sites.

Number	Site	Latitude (Degrees)	Longitude (Degrees)	Altitude (km)
1	Anmyeondo, Korea	36.54	126.33	0.03
2	Ascension Island	7.92	−14.33	0.03
3	Białystok, Poland	53.23	23.03	0.18
4	Bremen, Germany	53.10	8.85	0.03
5	Caltech, USA	34.14	−118.13	0.23
6	Darwin, Australia	−12.42	130.89	0.03
7	Edwards, USA	34.96	-117.88	0.70
8	Eureka, Canada	80.05	−86.42	0.61
9	Garmisch, Germany	47.48	11.06	0.74
10	Izaña, Tenerife	28.30	−16.50	2.37
11	Karlsruhe, Germany	49.10	8.44	0.12
12	Lamont, USA	36.60	−97.49	0.32
13	Lauder, New Zealand	−45.04	169.68	0.37
14	Ny Ålesund, Spitsbergen	78.90	11.90	0.02
15	Orléans, France	47.97	2.11	0.13
16	Park Falls, USA	45.95	−90.27	0.44
17	Paris, France	48.85	2.32	0.10
18	La Réunion Island, France	−20.90	55.49	0.09
19	Rikubetsu, Japan	43.46	143.77	0.36
20	Saga, Japan	33.24	130.29	0.01
21	Sodankylä, Finland	67.37	26.63	0.19
22	Tsukuba, Japan	36.05	140.12	0.03
23	Wollongong, Australia	−34.41	150.88	0.03

3   **Table 2.**   Past, future, and possible TCCON sites.

Number	Site	Latitude (Degrees)	Longitude (Degrees)	Altitude (km)
1	Arrival Heights, Antarctica	−77.83	166.66	0.25
2	Burgos, Philippines	18.50	120.85	0.10
3	East Trout Lake, Canada	54.35	-104.98	0.49
4	Four Corners, USA	36.80	-108.48	1.64
5	Manaus, Brazil	−3.10	−60.02	0.09
6	Oxfordshire, UK	51.57	-1.32	0.07
7	Paramaribo, Suriname	5.80	-55.20	0.05
8	Poker Flat, USA	65.12	-147.47	0.21
9	Yekaterinburg, Russia	57.04	59.55	0.30

Table 3. Averaged results of different colocation methods implemented for XCO_2 from NIES TM calculated for 16 TCCON sites. *The number of FLEXPART cells with resolution 1.0° × 1.0° is counted for methods based on the footprint (1–4), while for other methods NIES TM cells (2.5° × 2.5°) are used.

Case	Method of colocation	Mean number of cells*	Mean correlation coefficient	Absolute value of mean bias	Mean standard deviation
C1	Footprint limit $\log_{10}(x) = -0.5$	35	0.96	0.75	1.01
C2	Footprint limit $\log_{10}(x) = -1.0$	160	0.96	0.81	0.98
C3	Footprint limit $\log_{10}(x) = -1.5$	507	0.97	0.85	0.97
C4	Footprint limit $\log_{10}(x) = -2.0$	1071	0.97	0.88	0.96
C5	Within area of 2.5° × 2.5°	1	0.96	0.76	1.03
C6	Within area of ±5.0° × ±5.0°	16	0.96	0.79	1.00
C7	Within area of ±5.0° × ±10.0°	32	0.96	0.79	0.98
C8	Within area of ±7.5° × ±22.5°	108	0.97	0.80	0.97

Table 4. Averaged results of different colocation methods implemented for XCO_2 from the GOSAT ACOS product calculated for 16 TCCON sites.

Case	Method of colocation	Mean number of observations	Mean correlation coefficient	Absolute value of mean bias	Mean standard deviation
C1	Footprint limit $\log_{10}(x) = -0.5$	1190	0.93	0.65	1.18
C2	Footprint limit $\log_{10}(x) = -1.0$	3046	0.92	0.61	1.21
C3	Footprint limit $\log_{10}(x) = -1.5$	4880	0.93	0.62	1.15
C4	Footprint limit $\log_{10}(x) = -2.0$	6016	0.93	0.64	1.12
C5	Within area of 2.5° × 2.5°	976	0.93	0.81	1.11
C6	Within area of ±5.0° × ±5.0°	2042	0.92	0.67	1.19
C7	Within area of ±5.0° × ±10.0°	3111	0.92	0.65	1.19
C8	Within area of ±7.5° × ±22.5°	5002	0.93	0.64	1.16

Table 5. Averaged results of different colocation methods implemented for XCO_2 from the GOSAT NIES product calculated for 16 TCCON sites.

Case	Method of colocation	Mean number of observations	Mean correlation coefficient	Absolute value of mean bias	Mean standard deviation
C1	Footprint limit $\log_{10}(x) = -0.5$	1049	0.89	0.63	1.14
C2	Footprint limit $\log_{10}(x) = -1.0$	2890	0.92	0.52	1.20
C3	Footprint limit $\log_{10}(x) = -1.5$	4823	0.92	0.60	1.19
C4	Footprint limit $\log_{10}(x) = -2.0$	5922	0.92	0.56	1.16
C5	Within area of 2.5° × 2.5°	907	0.89	0.63	1.17
C6	Within area of ±5.0° × ±5.0°	1845	0.91	0.56	1.15
C7	Within area of ±5.0° × ±10.0°	2976	0.93	0.58	1.15
C8	Within area of ±7.5° × ±22.5°	4874	0.92	0.60	1.17

Table 6. Averaged results of different colocation methods implemented for XCO_2 from the GOSAT PPDF product calculated for 16 TCCON sites.

Case	Method of colocation	Mean number of observations	Mean correlation coefficient	Absolute value of mean bias	Mean standard deviation
C1	Footprint limit $\log_{10}(x) = -0.5$	357	0.84	0.50	1.11
C2	Footprint limit $\log_{10}(x) = -1.0$	870	0.86	0.62	1.12
C3	Footprint limit $\log_{10}(x) = -1.5$	1536	0.81	0.73	1.16
C4	Footprint limit $\log_{10}(x) = -2.0$	1911	0.81	0.67	1.17
C5	Within area of 2.5° × 2.5°	331	0.86	0.66	1.02
C6	Within area of ±5.0° × ±5.0°	749	0.85	0.64	1.15
C7	Within area of ±5.0° × ±10.0°	1114	0.83	0.69	1.19
C8	Within area of ±7.5° × ±22.5°	1733	0.86	0.68	1.17

Table 7. Averaged results of different colocation methods implemented for XCO_2 from the GOSAT RemoTeC product calculated for 16 TCCON sites.

Case	Method of colocation	Mean number of observations	Mean correlation coefficient	Absolute value of mean bias	Mean standard deviation
C1	Footprint limit $\log_{10}(x) = -0.5$	795	0.81	0.71	1.17
C2	Footprint limit $\log_{10}(x) = -1.0$	1898	0.83	0.66	1.19
C3	Footprint limit $\log_{10}(x) = -1.5$	3212	0.83	0.61	1.22
C4	Footprint limit $\log_{10}(x) = -2.0$	4091	0.83	0.59	1.21
C5	Within area of 2.5° × 2.5°	769	0.90	0.87	1.15
C6	Within area of ±5.0° × ±5.0°	1491	0.85	0.63	1.18
C7	Within area of ±5.0° × ±10.0°	2325	0.86	0.70	1.19
C8	Within area of ±7.5° × ±22.5°	3818	0.86	0.64	1.25

Table 8. Averaged results of different colocation methods implemented for XCO_2 from the GOSAT UoL-FP product calculated for 16 TCCON sites.

Case	Method of colocation	Mean number of observations	Mean correlation coefficient	Absolute value of mean bias	Mean standard deviation
C1	Footprint limit $\log_{10}(x) = -0.5$	634	0.88	0.78	1.31
C2	Footprint limit $\log_{10}(x) = -1.0$	1454	0.87	0.76	1.34
C3	Footprint limit $\log_{10}(x) = -1.5$	2450	0.88	0.80	1.28
C4	Footprint limit $\log_{10}(x) = -2.0$	3017	0.89	0.70	1.23
C5	Within area of 2.5° × 2.5°	629	0.86	0.73	1.33
C6	Within area of ±5.0° × ±5.0°	1215	0.88	0.76	1.30
C7	Within area of ±5.0° × ±10.0°	1852	0.86	0.74	1.27
C8	Within area of ±7.5° × ±22.5°	2799	0.85	0.72	1.25

Table 9. Comparison of colocation methods C4 versus C8 using ACOS, NIES, PPDF, RemoTeC, and UoL GOSAT products near the Darwin site.

GOSAT Product	Case	Correlation coefficient	Mean bias	Standard deviation	Number of observations
ACOS	C4	0.96	0.36	0.77	36292
	C8	0.94	0.50	0.90	10872
NIES	C4	0.94	0.09	0.88	26652
	C8	0.93	0.13	1.00	6924
PPDF	C4	0.70	0.24	1.02	13681
	C8	0.64	0.08	1.10	4333
RemoTeC	C4	0.91	0.44	0.95	23915
	C8	0.89	0.77	1.07	7130
UoL	C4	0.82	0.34	1.17	14376
	C8	0.86	0.17	1.10	4727

Table 10. Comparison of colocation methods C4 versus C8 using ACOS, NIES, RemoTeC, and UoL GOSAT products near the La Réunion site. The PPDF GOSAT product does not include any observations near the La Réunion site.

GOSAT Product	Case	Correlation coefficient	Mean bias	Standard deviation	Number of observations
ACOS	C4	0.82	0.70	0.83	11873
	C8	0.83	0.65	0.76	9640
NIES	C4	0.70	0.25	1.07	7720
	C8	0.73	0.45	1.02	6505
RemoTeC	C4	0.51	0.92	1.07	2482
	C8	0.61	1.16	1.04	3414
UoL	C4	0.45	0.75	0.94	860
	C8	0.36	0.71	1.00	2239
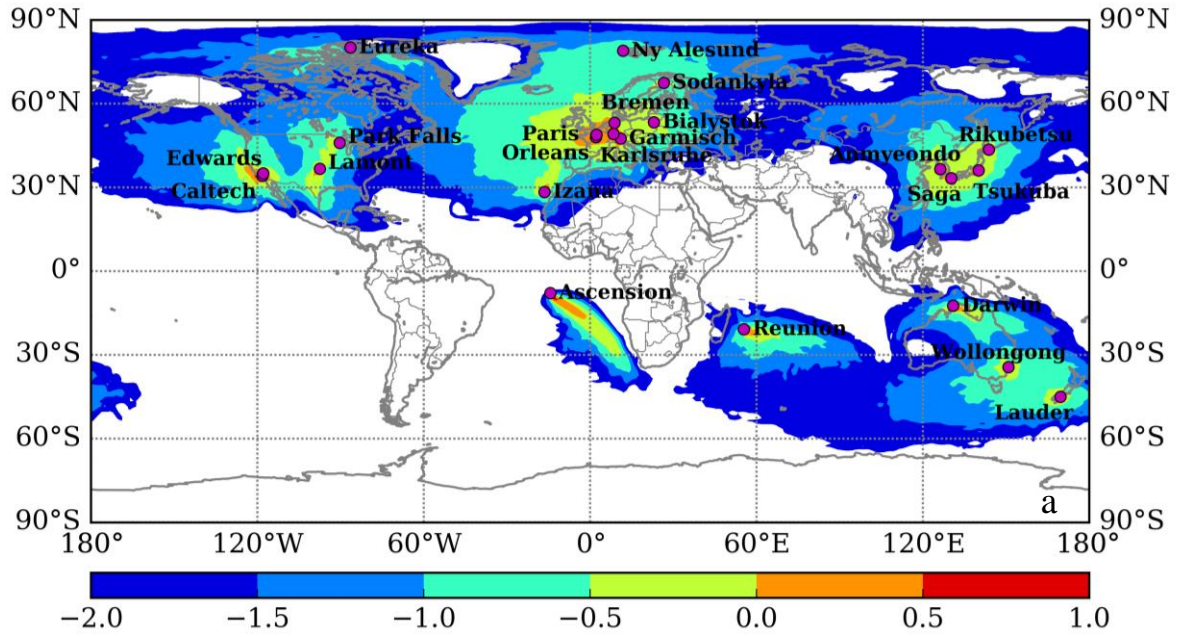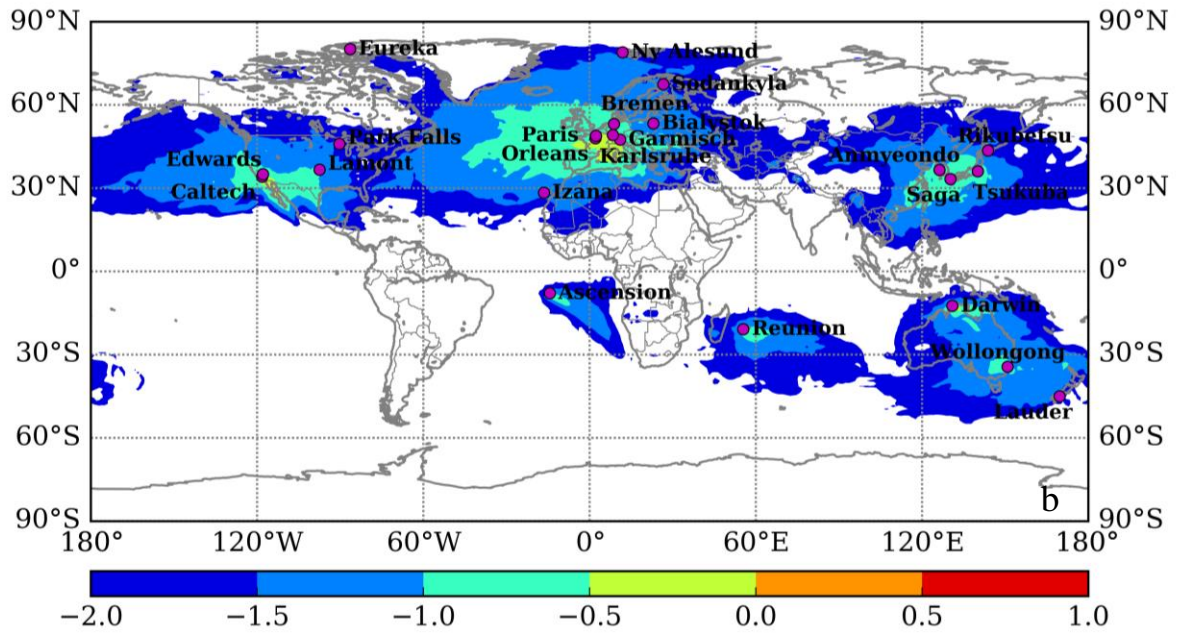
Fig. 1. Global distribution of the sensitivity of CO_2 concentrations (ppm (μmol $(m^2 s)^{-1})^{-1}$) with respect to the concentrations in adjacent cells, calculated using the FLEXPART model with a resolution of 1.0° for the 23 TCCON operational sites: a) tracer simulation initialized at the level of 1000 m, b) tracer simulation initialized at the level of 3000 m that corresponds to 700 hPa based on the International Standard Atmosphere for dry air.
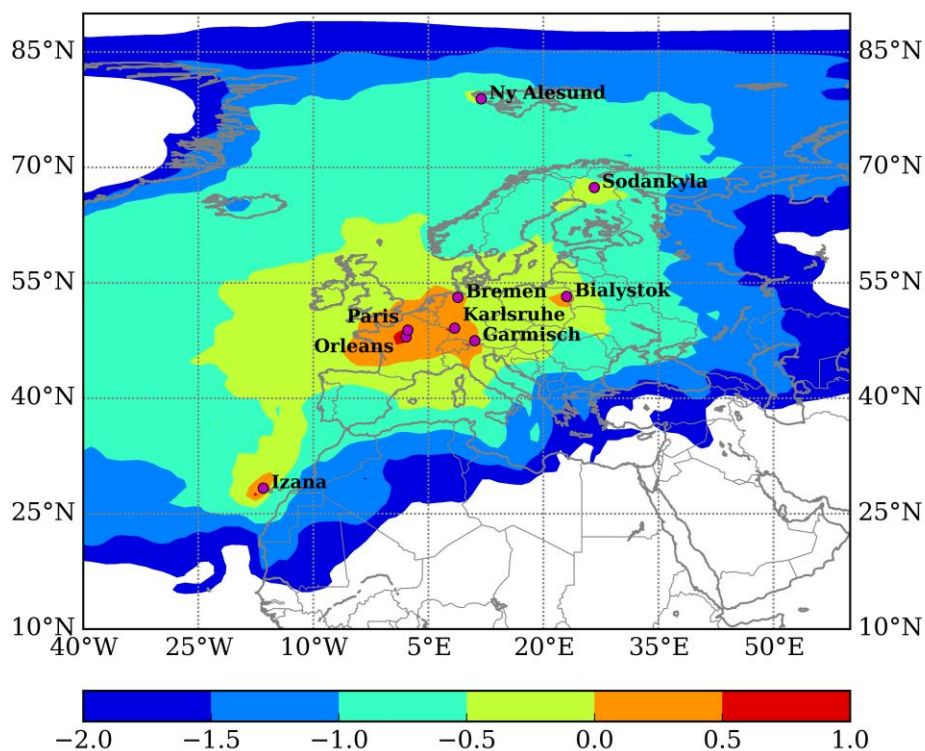
2 **Fig. 2.** Distribution of the sensitivity of CO_2 concentrations (ppm (μmol $(m^2s)^{-1})^{-1}$) in Europe with
3 respect to the concentrations in adjacent cells, calculated using the FLEXPART model with a
4 resolution of 1.0° for TCCON operational sites within Europe, using a tracer simulation
5 initialized at the level of 1000 m.
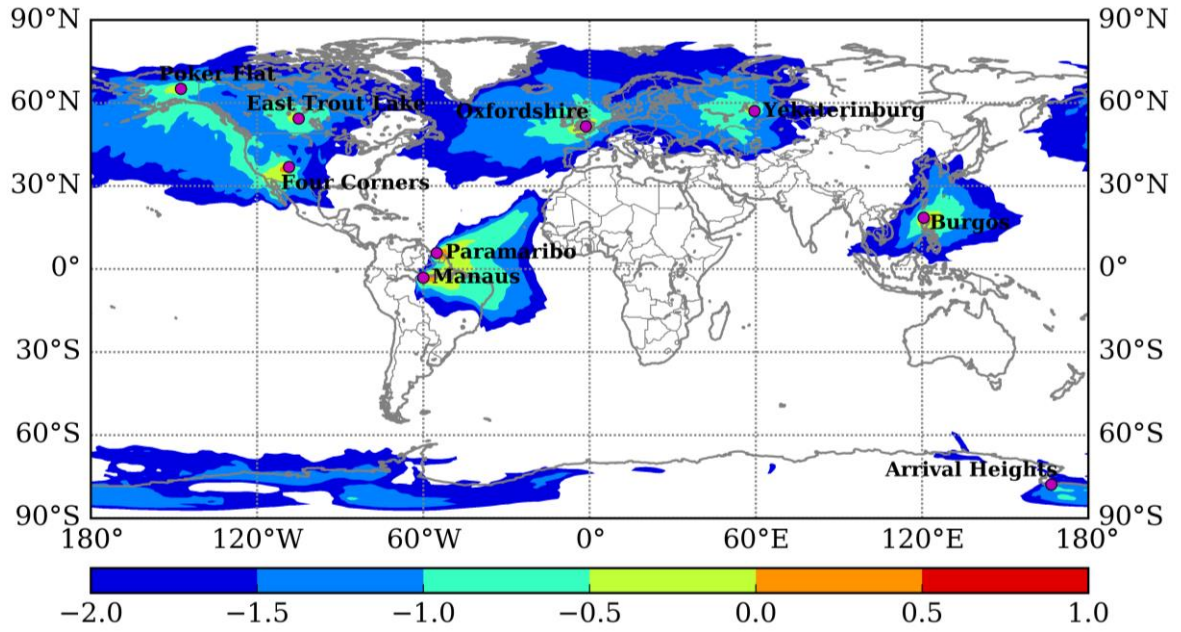
3   **Fig. 3.** Global distribution of the sensitivity of CO_2 concentrations (ppm (μmol (m^2s)$^{-1}$)$^{-1}$) with
4   respect to the concentrations in adjacent cells, calculated using the FLEXPART model with a
5   resolution of 1.0° for 9 past, future, and possible TCCON operational sites, using a tracer
6   simulation initialized at the level of 1000 m.
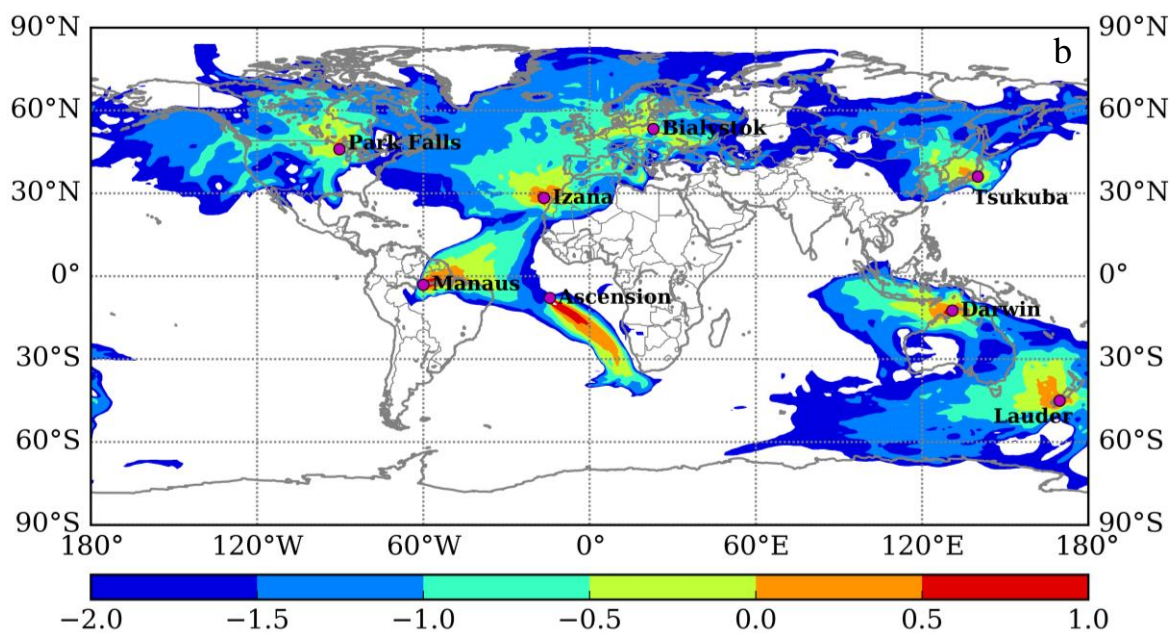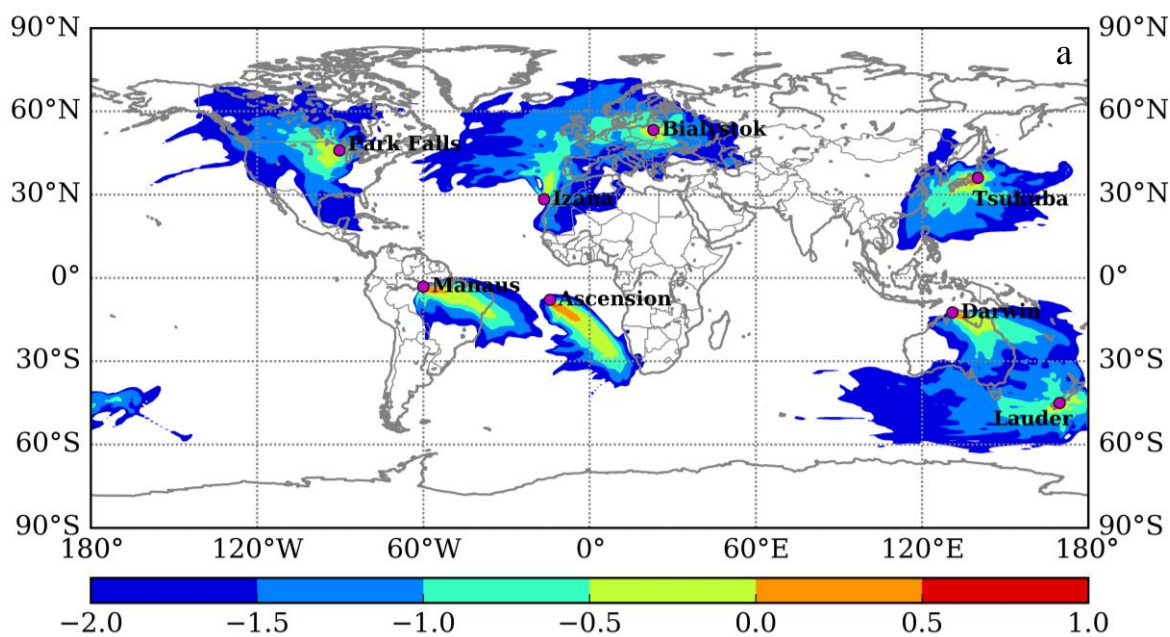
Fig. 4. Footprints for different seasons for Ascension Island, Białystok, Darwin, Izaña, Manaus, Park Falls, and Tsukuba, for a) the summer (June, July, and August) of 2010 and b) the winter (December, January, February) of 2010–2011.
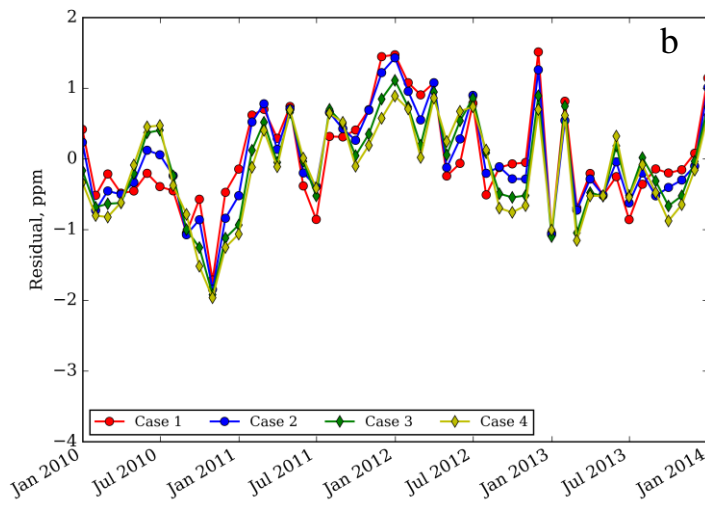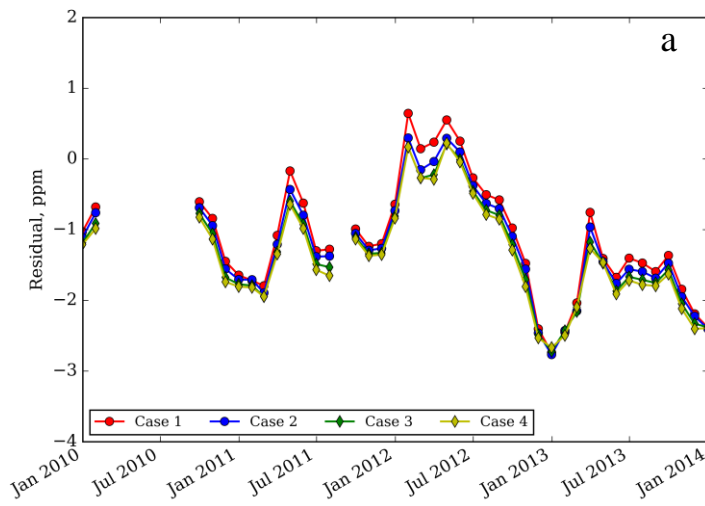
3 **Fig. 5.** Monthly average residuals of modeled XCO$_2$ compared with TCCON ground-based FTS for
4   methods C1, C4, C5 and C8, for a) Darwin and b) Garmisch.
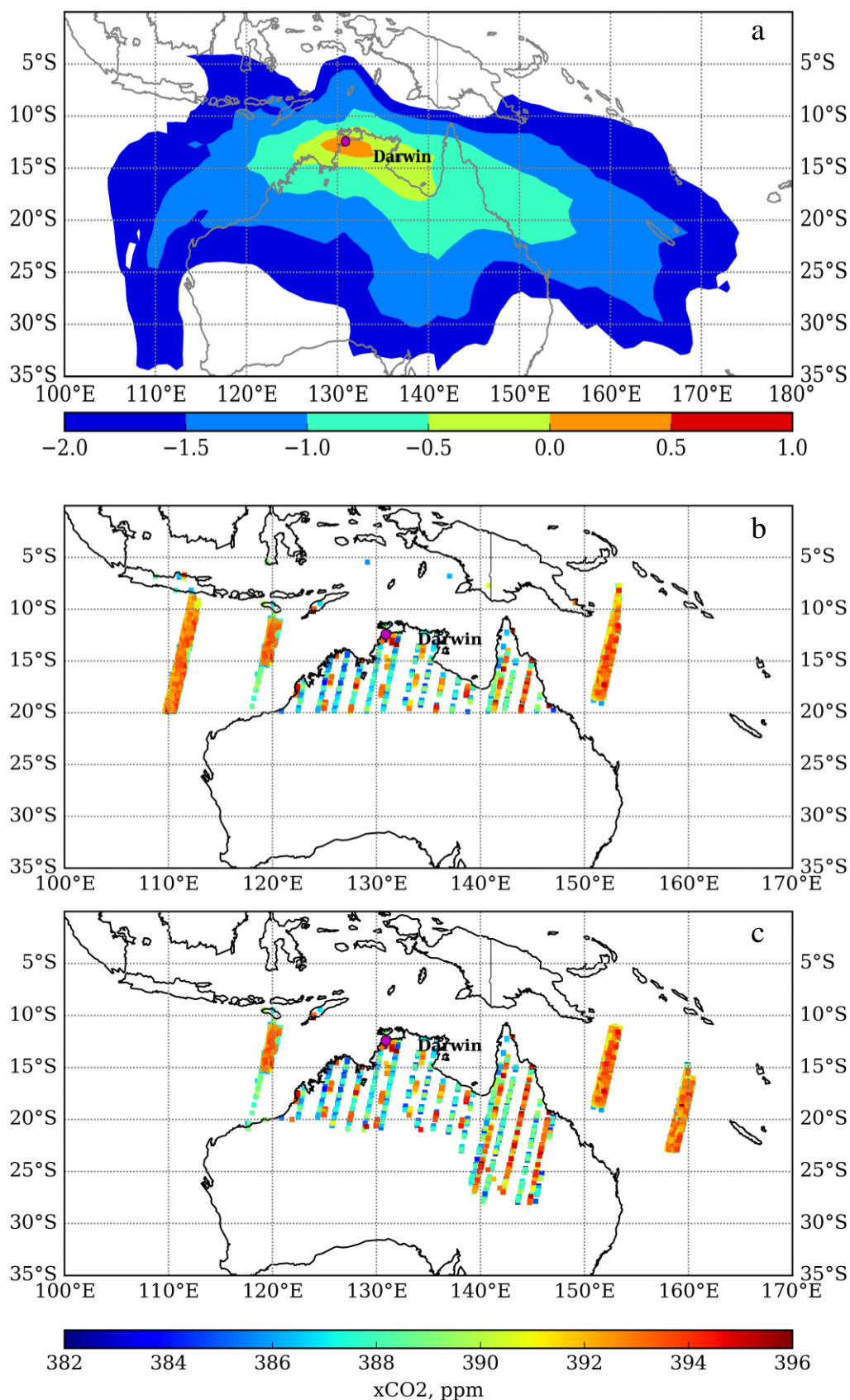
Fig. 6. a) Annual average footprint for the Darwin TCCON observation site; ACOS GOSAT XCO_2 observations selected using b) the geostatistical method within an area of $\pm 7.5° \times \pm 22.5°$, and c) the footprint-based method with the limit $\log_{10}(x) = -2.0$.
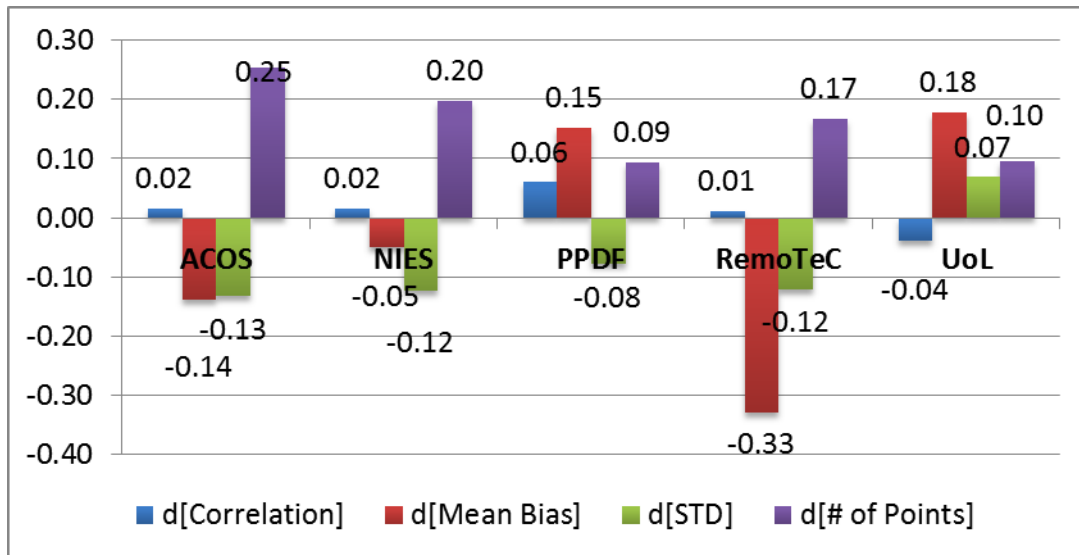
2 **Fig. 7.** Difference (denoted as d[]) in correlation coefficients, mean bias (ppm), STD (ppm) and
3   number of observational points between methods C4 (the colocation domain size is
4   determined by sensitivity values (ppm (μmol $(m^2 s)^{-1})^{-1}$) with the limit of $\log_{10}(x)$ equal to –
5   2.0) and C8 (the colocation domain size is rectangular with dimension ±7.5° × ±22.5°) using
6   ACOS, NIES, PPDF, RemoTeC, and UoL GOSAT products near the Darwin site. Please note
7   scale of number of observational points is 10^5.
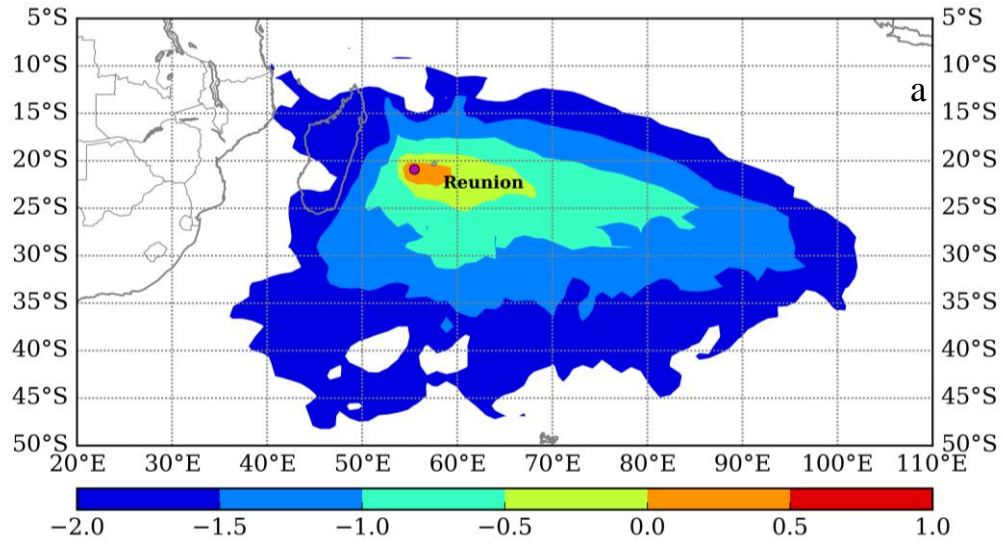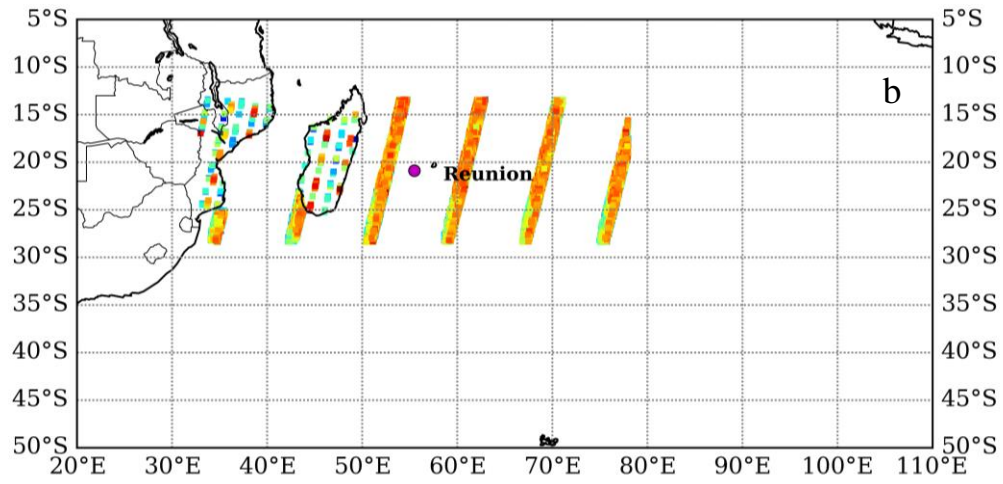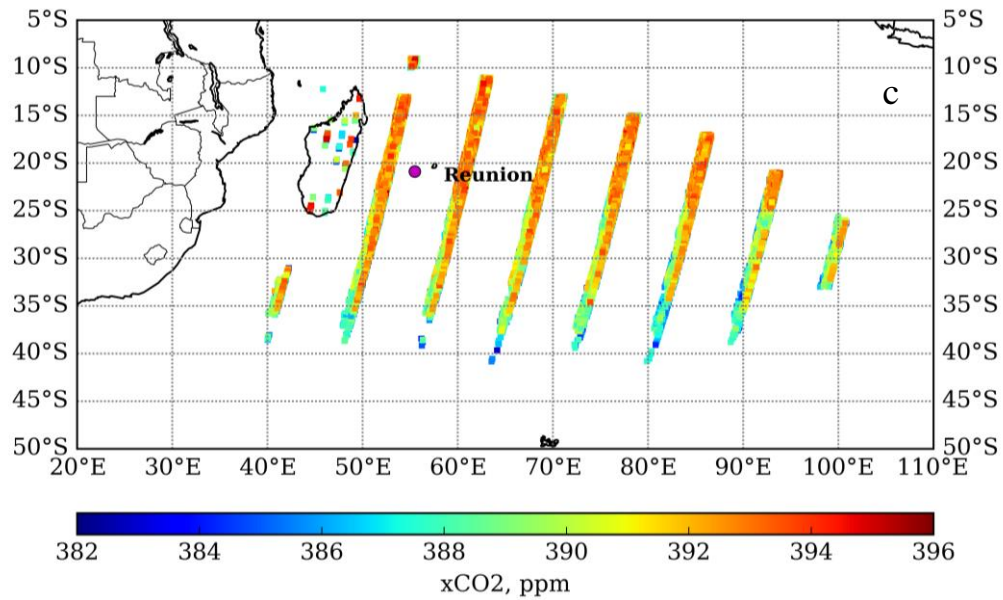
4   **Fig. 8.** a) Annual average footprint for the La Réunion TCCON observation site; ACOS GOSAT XCO$_2$
5   observations selected using b) the geostatistical method within an area of ±7.5° × ±22.5°,
6   and c) the footprint-based method with the limit log$_{10}$(x) = −2.0.

3 **Fig. 9.** UoL-FP GOSAT XCO$_2$ observations selected using a) the geostatistical method within an
4 area of ±7.5° × ±22.5°, and b) the footprint-based method with the limit $\log_{10}(x) = -2.0$.
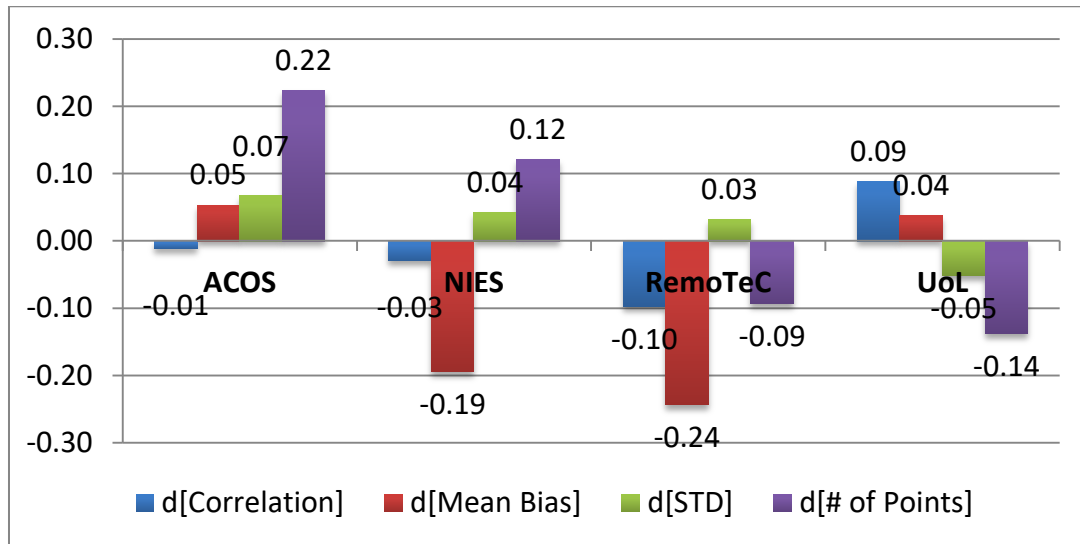
2   **Fig. 10.**   Difference (denoted as d[]) in correlation coefficients, mean bias (ppm), STD (ppm)
3   and number of observational points between methods C4 (the colocation domain size is
4   determined by sensitivity values (ppm (μmol $(m^2 s)^{-1})^{-1}$) with the limit of $\log_{10}(x)$ equal to −
5   2.0) and C8 (the colocation domain size is rectangular with dimension ±7.5° × ±22.5°) using
6   ACOS, NIES, RemoTeC, and UoL GOSAT products near the La Réunion site. Please note scale
7   of number of observational points is 10^4.